49th Lunar and Planetary Science Conference 2018 (LPI Contrib. No. 2083)

2104.pdf

SCRUTINIZING SIX SILICIDE-BEARING SAMPLES OF METAL FROM THE NORTON COUNTY

AUBRITE Laurence A.J. Garvie[1,2], Soumya Ray[2], Meenakshi Wadhwa[1,2], Axel Wittmann[3], and Kenneth Domanik[4] [1]Center for Meteorite Studies, [2]School of Earth and Space Exploration, Arizona State University, 781 East Terrace Rd., Tempe, AZ 85287-6004 (lgarvie@asu.edu). [3]LeRoy Eyring Center for Solid State Science, Arizona State University, Tempe, AZ 85287-1704. [4]Lunar and Planetary Laboratory, University of Arizona, Tucson, AZ 85721.

Introduction: Aubrites are igneous rocks dominated by brecciated pyroxenites that formed under highly reducing conditions [1]. Metal is typically present at the 0.1 to 1 % level, although to ~7% in Shallowater. The metal is typically Si-rich, with 0.12-2.44 wt% Si, though some grains in Norton County are Si-free [2,3]. Aubrites are thought to be related to enstatite chondrites, though the exact relationship is still debated.

Mineralogically, the aubrites are of interest since they equilibrated under such low oxygen-fugacity conditions, that normally lithophile elements became chalcophile. For example, Norton County contains oldhamite-dominated (CaS) lithic clasts with crystals to 2 cm [4]. Similarly, much of the Fe-Ni metal is Si bearing; this Si resides in the kamacite and in perryite, an Fe-Ni-P silicide [2, 5]

In our first study [3], we investigated six small (< 1 mm) Norton County metal nodules, four of which contain abundant silicides, and two of which are Si free. Here we extend this study by revealing the elemental, mineralogical, and petrographic characteristics of six large (> 6 mm to 20 mm) Norton County metal nodules. Particular emphasis is given to the precipitates and their composition, which can provide valuable information on the thermal history and formation of the metal.

Samples and preparation: Six metal nodules (NC7 to 12) were hand-picked from the Norton County aubrite. They ranged from 0.75 g to >13.3 g. Nodules NC7, 9, and 10 are spheres, whereas the others are irregularly shaped. Each sample was sectioned and one half embedded in a resin mount. The samples were polished, etched briefly in nital, and washed in water and methanol. The samples were analyzed with optical microscopy, and SEM imaging and WDS analysis were performed with the JEOL JXA-8530F Hyperprobe in the LeRoy Eyring Center for Solid State Science at ASU, and the CAMECA SX100 electron microprobe in the Michael J. Drake Electron Microprobe lab at UofA. Bulk WDS data were obtained by analyzing two perpendicular transects across each nodule. Each transect consisted of 100 points, with a 20-μm beam size.

Results: Each nodule has a distinct, though similar composition (Table 1), and excluding the large precipitates, similar bulk and kamacite compositions across each. Our elemental data is within the range of previous studies e.g., [2,6]. Kamacite Si and Ni contents are inversely linearly correlated ($R^2 = 0.92$). Taking into account the results from our first study [3], the kamacite analyses for the silicide-rich nodules range from 0.25 to 1.83 wt% Si. Phosphorous is near or below detection limit in the kamacite. The difference between the bulk and kamacite compositions is a reflection of the abundant silicides in the nodules.

The polished and etched surface of each sample is dominated by a pseudo-Widmanstätten pattern delineated by laths up to several mm long and up to 12 μm thick. The spherical nodules (NC7, 9, 10) are single crystals as evidenced by the pseudo-Widmanstätten patterns. The other nodules are polycrystalline with grain boundaries separated by perryite and schreibersite. Within the nodules, schreibersite was only found as isolated anhedral and large vermicular grains. Rare

Table 1. WDS bulk and kamacite compositions

Nodule		Fe	Si	P	Ni	Co	Ni/Co
NC7	*bulk**	*92.5*	*1.64*	*0.12*	*5.52*	*0.32*	*17.3*
	kamacite**	93.9	1.41	bdl	3.88	0.33	11.8
NC8	*bulk*	*91.7*	*1.40*	*0.10*	*6.54*	*0.28*	*23.4*
	kamacite	94.4	1.15	bdl	4.16	0.30	13.9
NC9	*bulk*	*91.4*	*2.12*	*0.07*	*6.33*	*0.33*	*19.2*
	kamacite	93.9	1.83	bdl	3.69	0.35	10.5
NC10	*bulk*	*90.6*	*1.75*	*0.06*	*6.67*	*0.35*	*19.1*
	kamacite	94.0	1.29	bdl	3.99	0.37	10.8
NC11	*bulk*	*91.8*	*0.62*	*0.10*	*6.88*	*0.33*	*20.9*
	kamacite	93.2	0.47	bdl	5.88	0.34	17.3
NC12	*bulk*	*90.5*	*0.73*	*0.10*	*8.10*	*0.30*	*27.0*
	kamacite	93.4	0.40	bdl	5.83	0.32	18.2

*mean of 200 points. ** mean of 50 points. bdl – below detection limit. Analyses in wt%.

daubréelite (containing Co and Zn) and caswellsilverite also occur. Graphite is relatively common occurring as irregularly shaped anhedral clusters.

Nodule NC12 contains a 1-mm-wide triangular plessitic region bordered by high Ni (48.1 wt%) that decreases to ~20 wt% near the center. Graphite flakes are common within the center. The rim is consistent with tetrataenite, with formula $Fe_{51.2}Cu_{0.4}Si_{1.5}Ni_{47.0}$ (in at%). The interior of the plessite exhibits a lath-like structure that compared to the surrounding material is dark under BSE imaging, though the Ni contents are similar. Though C-coated, EDX analysis of the darker laths show them to be significantly C-rich compared to the lighter-colored (in BSE) metal, suggesting an Fe-Ni carbide. The taenite has composition $Fe_{79.5}Co_{0.2}Si_{1.2}Ni_{19.1}$ (in at%), with Co instead of Cu. Two sides of the plessite triangle have embayed margins with each prominence attached to an anhedral perryite grain. The third side has a straight tetrataenite/kamacite boundary with

attached Ni-Fe silicide (Fig. 1). The silicides are described further below.

Silicides: Fe-Ni-Si-P precipitates are present in each nodule, prominently displayed on the polished surfaces as a pseudo-Widmanstätten pattern. These silicides have been identified as perryite [5,7], though accurate analysis is complicated by their typically <1-μm size and high Ni content. WDS of these small precipitates embedded in kamacite is problematic as the Ni Kα X-rays of the silicide excite Fe Kα X-rays from the surrounding kamacite matrix. As such, WDS analyses of the Ni-rich silicides significantly over estimate Fe contents giving totals of 103 wt% or greater. To overcome the fluorescence problem, the NC9 precipitates were extracted with nital and deposited onto a Be planchette. WDS of the larger flat grains gave totals ~100 wt%. The acid insoluble residue is dominated by Ni-Fe silicides comprised of flat plates of the long silicide laths, fried-egg-shaped grains, and rarer, small euhedral grains.

WDS analysis of the thick plates deposited on the Be planchette give Ni 81.9±0.8, Fe 1.00±0.1, Cu 0.35±0.02, Si 13.48±0.85, P 2.58±0.47 wt% (n=10); these values are within the published range, though the Fe content is lower [2]. The cation:anion ratio of perryite is variously published as 8:3 and 5:2. A single-crystal structure refinement of synthetic perryite [7] provides an ideal formula of $(Ni,Fe)_8(Si,P)_3$. Nickel silicides of the M_8X_3 type have not been observed in the Ni-Si system at 1 atm, suggesting that Fe and P are necessary to stabilize the structure [7]. The structural complexity of perryite arises from the stacking of "fundamental layers" of Ni with partial substitution by Fe, and Si with partial substitution by P: these layers stack along the c axis. Thus, the synthetic perryite [7] is isomorphous with Pd_8Sb_3, which is a stacking variant of $Ni_{31}Si_{12}$ and Pd_5Sb_2 structures. More recent studies of Ni-Si phase relations [8] suggest that $Ni_{31}Si_{12}$ is the stable composition, and not the M_8X_3 or M_5X_2 compositions. Our Norton County data for large NC9 plates give an empirical formula based on Si+P=12 of

$(Ni_{29.71}Fe_{0.38}Cu_{0.12})_{\Sigma=30.2}(Si_{10.22}P_{1.78})_{\Sigma=12}$
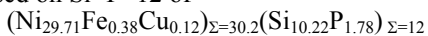
While the large plates show a narrow compositional range, the small euhedral precipitates typically show higher Cu and Fe and lower P. For example, a 5 μm euhedral precipitate has the empirical formula based on Si+P=12 of

$(Ni_{29.78}Fe_{0.94}Cu_{0.19})_{\Sigma=30.9}(Si_{11.74}P_{0.26})_{\Sigma=12}$
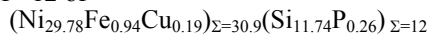
which is within error the same stoichiometry as the $Ni_{31}Si_{12}$ phase.

In addition to perryite, five P-free Ni-Fe-Si precipitates are attached to the tetrataenite of the plessite in NC12 (Fig. 1). The largest grain is euhedral and ~10 x 4 μm. WDS analysis of this grain shows Ni 84.9 wt%, Fe 5.7 wt%, Cu 0.2 wt%, and Si 12.7 wt%. Based on anion content of 12, the cation:anion ratio is 41:12 and inconsistent with the $Ni_{31}Si_{12}$ structure. The Si content of ~23 at% is similar to that of Ni_3Si [8-10]. Based on Si=2, this ternary phase has the composition $(Ni_{6.4}Fe_{0.5})_{\Sigma=7}Si_2$. This precipitate may represent the Ni

analogue of suessite, $(Fe,Ni)_3Si$, and as such is a new mineral.

Discussion: This study extends our knowledge of the metallography of the silicide-rich metal nodules in Norton County. The new ternary precipitate $(Ni_{6.4}Fe_{0.5})_{\Sigma=7}Si_2$ requires further investigation as no such phase is shown in the isothermal section of the Fe-Ni-Si system at 850°C [9,10]. However, Fe is soluble in the β_1-Ni_3Si phase up to 7.6 at% [9,10], with the Norton County phase containing 5.1 at% Fe, suggesting that the ternary phase is related to β_1-Ni_3Si.
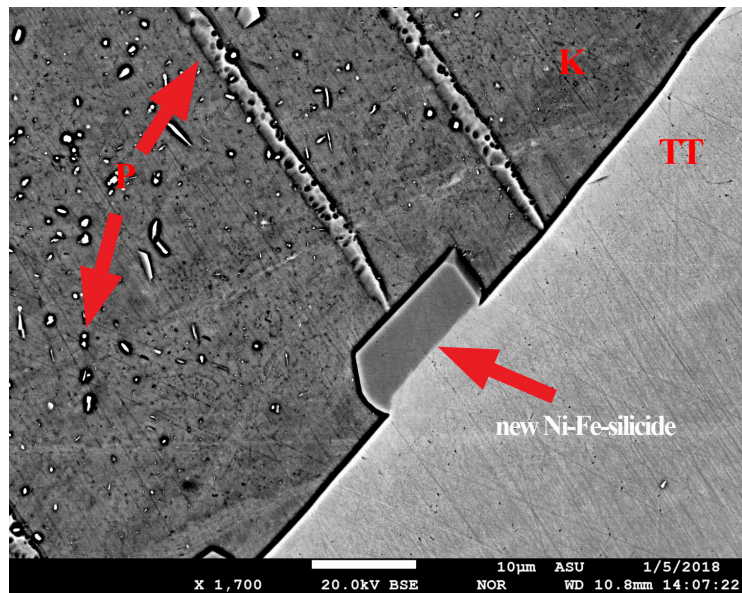

Figure 1. BSE image of a portion of NC12 showing the new Ni-Fe silicide attached to tetrataenite (TT). K - kamacite and P - perryite.

We provide here an updated and consistent empirical formula for perryite, which is based on the $M_{31}X_{12}$ stoichiometry. Okada et al. [11], suggest the existence of two distinct populations of perryite in Norton County based on their Fe contents, whereas this was later refuted [2]. Our data does show compositional differences between the large perryite laths that define the pseudo-Widmanstätten pattern and the smaller euhedral grains that crystallized within the trapezoidal regions defined by the laths. However, further work is needed to see if this relationship holds for the other nodules.

References: [1] Mittlefehldt et al. (1998) in Rev. Mineral. **36**, 4-1-4-195. [2] Casanova et al. (1993) GCA, **57**, 675-682. [3] Garvie et al. (2017) 80th Met. Soc., abstract #6384. [4] Wheelock et al. (1994) GCA, **58**, 449-458. [5] Wai (1970) Min Mag, **37**, 905-908. [6] Lyul' et al. (2013) Geochem Internat **51**, 777-791. [7] Okada et al. (1991) Acta Cryst **C47**, 1358-1361. [8] Connétable and Thomas (2011) J. Alloys Comp **509**, 2639-2644. [9] Ackerbauer et al. (2009) Intermetallics, 17, 414-420. [10] Zhang et al. (2009) J Alloys Comp **481**, 509-514. [11] Okada et al. (1988) Meteoritics, **23**, 59-74.